



HAL
open science

Geophysical signature of the transition zone between the sedimentary cover and the basement from an analogue of the Rhine Graben

François Bretaudeau, Mathieu Darnet, J. Porté, Catherine Lerouge, Samantha Neeb, J.F. Girard, Jean-Michel Baltassat, Nicolas Coppo, Y. Lucas, Chrystel Dezayes

► To cite this version:

François Bretaudeau, Mathieu Darnet, J. Porté, Catherine Lerouge, Samantha Neeb, et al.. Geophysical signature of the transition zone between the sedimentary cover and the basement from an analogue of the Rhine Graben. *Geothermics*, 2022, 102, pp.102356. 10.1016/j.geothermics.2022.102356 . hal-03687189

HAL Id: hal-03687189

<https://brgm.hal.science/hal-03687189>

Submitted on 22 Jul 2024

HAL is a multi-disciplinary open access archive for the deposit and dissemination of scientific research documents, whether they are published or not. The documents may come from teaching and research institutions in France or abroad, or from public or private research centers.

L'archive ouverte pluridisciplinaire **HAL**, est destinée au dépôt et à la diffusion de documents scientifiques de niveau recherche, publiés ou non, émanant des établissements d'enseignement et de recherche français ou étrangers, des laboratoires publics ou privés.



Distributed under a Creative Commons Attribution - NonCommercial 4.0 International License

Geophysical signature of the transition zone between the sedimentary cover and the basement from an analogue of the Rhine Graben

F. Bretaudeau^a, M. Darnet^a, J. Porté^{a,b}, C. Lerouge^a, S. Neeb^a, J.F. Girard^b,
J.M. Baltassat^a, N. Coppo^a, Y. Lucas^c, C. Dezayes^a

^a*BRGM, Orléans, FRANCE*

^b*EOST-IPGS, Strasbourg University, FRANCE*

^c*EOST-LHyGeS, Strasbourg University, FRANCE*

Abstract

Exploiting high temperatures geothermal resources in sedimentary and basement rocks, rifts or flexural basins to produce electricity is now possible because of the development of binary geothermal power plant technology. However it remains challenging because the presence of fluid and permeability at 4-5km depth is necessary. A multi-scale and multi-disciplinary approach to increase our knowledge of the transition zone between the sedimentary cover and the basement have been undertaken to provide fundamental knowledge for the assessment of its geothermal potential. In this paper, we report out the results of a study performed on an exhumed transition zone in the Ringelbach area in the Vosges Mountain, on the flank of the Rhine graben. In this analogue of a deeply buried transition zone of the Rhine Graben, Triassic sandstones are still present on the top of the fractured and altered granitic basement providing the unique opportunity to study in-situ the physical properties of this transition zone. We focused here on electrical and seismic properties of the transition zone as they are the main physical parameters usually assessed with the help of geophysical methods during the exploration phase of a geothermal project.

We show that altered porous and potentially permeable granite targeted in deep geothermal exploration has a clear signature on both electrical conductivity and seismic measurements that can be measured at core scale, borehole scale, and are still visible with surface geophysical methods such as refraction and reflec-

tion seismic and Controlled Source Electromagnetism at a few hundred meter depth. The results suggest that best discrimination between permeable and non permeable rocks may be provided by the joint interpretation of both resistivity and seismic velocities.

Keywords: Geophysical exploration, Seismic, Controlled-Source Electro-magnetic, Magnetotelluric, Rhine Graben, Ringelbach, transition zone

1. Introduction

Exploiting geothermal resources at temperatures between 120 and 200°C in sedimentary and basement rocks, in rifts or in flexural basins, to produce electricity is now possible because of the development of binary geothermal power plant technology. Reaching such temperature range is a major challenge for
5 mainland France and Europe as it usually requires drilling up to 4 to 6 km depth. Aside from temperature, two other conditions are required to allow the exploitation of the geothermal energy: the presence of fluid, which is the heat vector, and sufficient permeability to allow the production and re-injection of
10 the fluid. This translates into the reservoir being located in the deep layers of sedimentary basins and the upper part of the Paleozoic basement, including the transition zone between the two.

The reality is however even more complex as the geothermal potential of this zone is also strongly influenced by large heterogeneities comprising 1) the lithol-
15 ogy/mineralogy of the cover/basement, 2) the internal architecture of the transition zone, 3) the anisotropic or heterogeneous cooling history of the batholith, degree of paleoalteration, and evolution of hydrothermalism and 4) the presence of natural faults and fracture networks above and below the transition zone. It is therefore clear that the characterization of the transition zone and its het-
20 erogeneity in the deeper part of sedimentary basins constitutes one of the most challenging problems for the development of geothermal resources.

Geophysical prospection methods such as 3D seismic reflection [1, 2] and Magnetotellurics [3, 4, 5] or Controlled-Source Electromagnetics [6, 7, 8, 9] are

commonly used to provide both structural and physical information at several kilometers depth. Those methods should help identifying favorable areas and de-risking geothermal projects. However, although a few authors have been interested in the impact of fracturing and hydrothermal alteration on seismic properties in the laboratory [10], it is not clear yet what would be the geophysical signature of the most permeable areas of the transition zone in terms of seismic or electrical properties.

We have undertaken a multi-scale and multi-disciplinary approach to increase our knowledge of this transition zone between the sedimentary cover and the basement and provide fundamental knowledge for the assessment of its geothermal potential. In this paper, we report out the results of a geophysical study performed in the Ringelbach site on an exhumed transition zone in the Vosges Mountain, on the flank of the Rhine graben. We focused on electrical and seismic properties of the transition zone as they are the main physical parameters usually assessed with the help of geophysical methods during the exploration phase of a geothermal project. We describe in a first part the Ringelbach analogue site, then present both seismic and electrical resistivity measurements collected at core scale, from borehole data, and then at the field scale. We finally discuss how those result may be extrapolated at larger depth.

2. Geological setting

Since 1975, the Ringelbach catchment has been the subject of interdisciplinary research on the major components of the temperate mid-mountain water cycle [11, 12, 13, 14]. The Ringelbach site is located on the eastern side of the Vosges Massif (NE France) (Figure 1) and consists of Hercynian porphyritic granite capped in its upper part by a residual cover of Triassic sandstones. The main granite is the medium-grained and porphyritic “granite des Crêtes” which consists of quartz, plagioclase, K-feldspar, biotite, and amphibole with minor titanite [15]. The Triassic sandstone cover, which gently dips towards the north,

is heterogeneous, formed by thick, hard medium-grained sandstone interstratified with a series of thin quartz-silty clay layers.

55 Two boreholes (F-HUR, F-HEI) were drilled within the area for hydrogeological purpose (Figure 1) ; the F-HEI borehole was doubled in its upper part (F-HEI, F-HEI2). Their detailed lithological and petrological descriptions are given in [15] and summarized in Figure 2. Neither of the two 150-m deep boreholes (F-HUR, F-HEI) reach the fresh granite. These two boreholes in-
60 dicate that sandstone in the top of the Ringelbach site covers a saprolite of several meters thick developed on granite and characterized by entire alteration of ferroan-magnesian minerals liberating iron and of plagioclase to form clays and iron-hydroxides. The thickness of the saprolite varies with the boreholes: 20 m in the FHUR borehole and 35 m in the FHEI borehole. The induration of
65 the saprolite increases toward its bottom. Underneath is a very thick layer of fractured and altered granitic bedrock. This succession of subhorizontal layers is interpreted as a truncated pre-Triassic stratified weathering profile of the Hercynian granite [15], as also proposed for other European Hercynian regions [16]. Several faults divide the basin into two main blocks (Hurlin, and Heidenkopf),
70 which are delimited by N30°E fault and progressively downthrown from southeast to northwest (Figure 1). A third block, in the southern part of the area, is delimited by a N80°E fault dipping to the North and is higher than the others.

3. Fracturation and water/rock alterations

Granites and their Triassic cover do not well outcrop. Triassic sandstones
75 that outcrop at the top of the hill near the F-HUR borehole (Hurlin block), occur as reddish medium- to fine-grained sandstones containing some pebbles and crosscut by mm- to cm-thick fractures partially filled by euhedral quartz and minor barite. Under the microscope, sandstones are essentially formed of monocrystalline quartz with minor K-feldspar, polycrystalline quartz, lithic
80 elements, largely cemented by at least two generations of authigenic quartz : a first generation of aureole quartz, and a second one sealing most of the residual

porosity. It is noteworthy that quartz filling fractures is luminescent, what is not the case of the two generations of quartz cements in the sandstone matrix. This difference of luminescence in quartz is related to the presence of trace elements
85 that are not currently known. However this demonstrates that quartz filling fractures and quartz cements in matrix precipitated from different fluids. The *granite des Crêtes* rather well outcrops on the middle slope of the hill, and has a quite fresh aspect. Weathering is marked by alteration of amphibole and of plagioclase cores. In the two boreholes, granite is highly affected by sub-vertical
90 fractures. The general paragenetic sequence of fracture fillings and wallrock alteration provide evidence of an early cataclasis stage associated with micro-quartz cementation followed by different generations of carbonates including calcite, dolomite and (Fe, Mn) - bearing dolomite, and barite.

4. Electrical properties

95 4.1. Core-scale measurements

Electrical formation factor and surface conductivity measurements have been performed on Ringelbach's granitic core samples taken from the F-HUR and F-HEI wells [17]. It shows that the higher porosity, the higher surface and pore fluid conductivity are (Figure 3). Since the amount of alteration clays controls
100 the rock surface conductivity [18], we can conclude that the higher the degree of alteration of the granite is, the higher the conductivity is. In addition, the higher the porosity is, the higher the permeability of the samples is (Figure 4). Porous and permeable altered granitic formations found within the transition zone are therefore likely to exhibit elevated electrical conductivity compared to
105 unaltered and tight granite.

4.2. Borehole logging

Figure 2 displays the logged resistivity data in the F-HUR well. Resistivity logs show overall high values (> 250 Ohm.m) over the crystalline basement but also a high degree of variability (250 – 6000 Ohm.m) caused by variations in

110 the degree of alteration/fracturing of the granite, as evidenced by the strong
correlation between resistivity readings and the rock competency. The close
relationship between elevated porosity/permeability and high electrical conduc-
tivity observed at the core scale can therefore be scaled up in the transition zone
to the size of the logging spatial sampling (metric to decametric scale).

115 4.3. Field scale CSEM measurements

To characterize the large-scale electrical resistivity distribution of the transi-
tion zone, we acquired a 3D Controlled Source Electro-Magnetic (CSEM) survey
over a 1000m x 1000m area cutting through the transition zone (from the Tri-
assic sedimentary cover deep down into the crystalline basement). Metronix
120 ADU stations were deployed on 50 sounding sites every 100m on a regular grid
to record both components of the horizontal electric field. Due to the very high
shallow resistivities, galvanic transmitters were not efficient so an $100000m^2$
horizontal transmitting loop located 1.5km from the receiver array was used
instead (Figure 5). Square signals with fundamental frequencies ranging from
125 0.25Hz to 8192Hz were injected in the loop using a 22kW TXM22 transmit-
ter, rising a current of 40A at 560V. Current in the loop and electric fields at
the stations are recorded simultaneously with GPS synchronisation. Accurate
position and orientations of each station electrodes as well as the transmitting
loop position are recorded using differential GPS in order to be considered ac-
130 curately in the 3D modeling process. After editing the data, a proper signal
deconvolution is achieved by computing the transfer functions between electric
fields and injected currents at each discrete frequency used. Transfer functions
are calculated using Razorback robust processing software [19, 20] in order to
remove incoherent noise. Analysis of the spectrum of the electric field transfer
135 function conducted to select for inversion 5 frequencies in the range 32Hz to
8192Hz for which the electric field varies significantly, highlighting sensitivity to
the underground resistivity variations. Due to the orientation of the transmit-
ter, east-west electric field component is largely dominant so north-south is weak
enough to be neglected. The selected data are inverted in 3D with POLYEM3D

140 software [21, 22, 23]. This code is a 3D massively parallel electromagnetic mod-
eling and imaging software dedicated to the inversion of CSEM and MT data.
The forward modeling relies on a frequency-domain secondary-field formulation,
a finite-difference discretization of Maxwell equations on an irregular cartesian
grid [24], and is solved using a direct solver. For this inversion, a 3D modeling
145 mesh of 700,000 cells is built with a dense core domain with 30m horizontal
spacing and 20m minimum vertical spacing up to 900m. The inverse problem is
solved using a linearized Gauss-Newton or quasi-Newton optimization method
[25]. Real and imaginary parts of the electric field at the 5 selected frequencies
are inverted. Parameterization and regularization are achieved here by using a
150 projection of the gradient of the data misfit function on smooth basis functions
designed to describe appropriately the inversion domain. The inversion domain
is also limited to the area covered with the receiver stations. The inversion is
also preconditioned with an arbitrary function to compensate the loss of sensi-
tivity with depth [26] and reduce sensitivity singularity due to single source
155 illumination. Each inversion run with this mesh lasts typically a few hours on
the CINES Bull supercomputer Occigen on 256 MPI processes for a few tenths
iterations depending on the regularisation and optimisation technique used.

We start inversion with a very rough initial guess using an homogeneous
160 half space at $2000 \Omega.m$. Data fit is good, reducing the RMS residuals from
518% in the starting model to 38%. Real and imaginary parts of electric field
for observed data and computed in the homogeneous half space and the final
inverted model are presented for a few representative stations Figure 6. The
very weak variation at low frequency suggests a low sensitivity of the lowest
165 frequencies to large depth structure. However more significant variations at
high frequencies show very good fit with both real and imaginary parts. Hor-
izontal slices at several depth as well as S-N and W-E profiles extracted from
the final 3D resistivity cube are shown Figures 7 and 8 respectively. Slices are
compared figure 7 with the current geological map of the area with the known
170 fault. The surface resistivity extracted from interpolated ERT profiles of [27] is

also presented. The 3D model is probably slightly distorted and preferentially stretched N-S due to the asymmetrical illumination obtained with the use of the single transmitter located North. The model shows high overall resistivities but also very high contrasts, ranging between $300 \Omega.m$ to more than $3000\Omega.m$. At shallow depths, high resistivity values ($3000\Omega.m$) are located in the southern part of the survey area, well delineated, and corresponds well to the very resistive anomaly imaged by ERT profiles in [27]. This resistive body is about 100m thick. It also matches to the higher granitic block delimited by the N80°E fault and the both N30°E faults (Figures 7). The resistive anomaly associated to fresh granite disappears at depths greater than 100m (Figures 8a). Beside the resistive block and everywhere below 100m, the model shows a conductive layer associated with altered and fractured zones that extends well over more than 200m depth into the basement and is laterally extensive. Beyond 300m depth, resistivity gradually increase to reach at large depth the high resistivities of fresh granite (Figures 8b) about $3000\Omega.m$. The E-W cross-section shows the shallow high resistivity to 100-200m depth separated by two more conductive zones (Figures 8b). Theses zones match with the both N30°E fault delimiting the Hurlin block. Those variations suggest that the thickness of this conductive zone to the base of the sedimentary cover varies laterally (from zero to 200m depth), most likely due to a different alteration history and intensity of the granite. Those results show that the resistivity variations due to alteration observed at core and borehole scale are also visible at the field scale where it still exhibits contrasts of at least one order of magnitude between fresh and altered granite.

5. Seismic properties

5.1. Core-scale measurements

P-wave velocities measurements (Figure 3) have been performed on Ringelbach's core samples taken from the F-HUR and F-HEI wells [17]. It shows that the higher porosity, the lower the P-wave velocity is. As for the electrical con-

200 ductivity, we can therefore expect that porous and permeable altered granitic
formations found within the transition zone exhibit lower P-wave velocity com-
pared to unaltered and tight granite.

5.2. Borehole logging

Figure 2 displays the logged sonic velocities in the F-HUR well. Sonic logs
205 show overall high values (> 4500 m/s) over the crystalline basement but also a
high degree of variability ($3000 - 5500$ m/s) caused by variations in the degree
of alteration/fracturing of the granite, as evidenced by the strong correlation
between sonic readings and the rock competency. The close relationship between
elevated porosity/permeability and low P-wave velocity in the transition zone
210 observed at the core scale (Figure 3) can therefore be up-scaled at least to the
size of the logging spatial sampling (metric to decametric scale).

5.3. Field scale seismic measurements

To characterize the large-scale P-wave velocity distribution of the transition
zone, we acquired a 1100m long seismic refraction/reflection profile over the
215 Triassic sedimentary cover cutting through three fault zones identified in the
area (figure 5). We used a 240 geophones array with 5m spacing and a shot every
10m operated with a 3000 Joules AP200 accelerated impact energy source. A 2D
first arrival travelttime tomography inversion was performed. On the other hand,
the same dataset was used to produced a high resolution reflection profile with
220 constant velocity migration. Tomography and migrated reflection profile are
represented Figure 9. Very high P-wave velocities are imaged, rising 4000-5000
m/s at larger depths and close to 2000 m/s in the first tenths meters. A clear
velocity drop from 4000-5000 m/s down to 3500-4000 m/s is observed at the top
of the crystalline basement (within the first 100m) when crossing these faults
225 (Figure 9). Interestingly, numerous and continuous reflectors are clearly visible
on the reflection profile at about 200m depth. Those reflectors obviously present
within the basement are possibly caused by some layering in the alteration, as
evidenced by the layering observed on the sonic logs in the exploratory boreholes,

or by a sharp transition between the end of the transition zone and the top of
 230 the fresh granite. On the other hand, those reflectors fade away when crossing
 the fault zones identified both by surface geology and velocity drop in the P-
 wave tomography, possibly indicating the presence of more strongly altered and
 fractured granite above the fault zones. Here again, those variations suggest that
 the thickness of the transition zone varies laterally (from 100 to 200m depth),
 235 most likely due to a different fracturation and alteration history in the granite.
 Those results show that the seismic variations due to alteration observed at
 core and borehole scale are also clearly visible at the field scale with possible
 contrasts of 30% between fresh and altered granite.

6. Discussion

240 6.1. Surface versus pore electrical conductivity

Waxman and Smits' (1968) equation [28] can be used to describe the rela-
 tionship between surface, pore and total electrical conductivity of a clay-rich
 porous media as follows:

$$\sigma_0 = \frac{\sigma_w}{F} + \sigma_s \quad (1)$$

with σ_0 the rock conductivity, σ_s the surface conductivity, σ_w the fluid conduc-
 245 tivity and F the rock formation factor.

We computed the total rock conductivity at 10 and 200°C as function of the
 fluid salinity for altered and unaltered Ringelbach granite (Figure 10) using Sen
 and Goode (1992) relationship [29] for the brine conductivity and the following
 constants derived from the core sample analysis:

	Porosity	Formation Factor	Surface Conduction	Permeability
Fresh granite	1.8%	1900	2.3 mS/m	10^{-18} m^2
Altered granite	5.3%	480	20 mS/m	10^{-16} m^2

250

The less saline/colder the fluid, the more important the surface conduction is.
 For the Ringelbach case, groundwater in the surface boreholes is fresh (salinity
 $\sim 100 \text{ mg/L}$) and as a consequence, the total conductivity of the granite is

mainly due to surface conduction and hence a proxy of mineral alteration but
255 not indicative of rock porosity. Conversely, the more saline/hotter the fluid, the
more important pore fluid conduction is. For deep and hot geothermal brines
like found in Soultz-sous-Forêts in the Rhine graben (salinity of 100 g/L and
temperature of 200°C), pore fluid conductivity is dominating and the total rock
conductivity is indicative of the rock porosity and hence potentially a proxy of
260 the rock permeability.

6.2. *Electrical and seismic properties of deep geothermal reservoirs*

To validate the aforementioned electrical conductivity model for deep geother-
mal reservoirs, we present here electrical resistivity measurements made in the
Soultz-sous-Forêts granitic basement (Figure 11). As predicted, altered zones
265 are electrically more conductive than unaltered granite, with a factor ranging
from ten to thousand times. Similarly, in the Rittershoffen geothermal project,
altered zones at the top of the granitic basement proved to be electrically con-
ductive but notably, the main permeable fault zones coincide with the most
electrically conductive zones [30]. The electrical conductivity of the granitic
270 basement is therefore a parameter of choice to explore for deep porous and
potentially permeable fault zones. The challenge remains to deploy electro-
magnetic techniques capable of remotely detecting and imaging such anomalies,
deeply buried underneath a thick sedimentary cover.

On seismic measurements, the most altered zones within the basement in Soultz-
275 sous-Forêts show significant decrease in P-wave and S-wave velocities (up to
30%). However, the less altered zones do not exhibit any significant anom-
alies, most likely due to the limited sensitivity of elastic properties to alteration.
To compensate for that, a joint analysis of electrical and elastic properties is
necessary. Indeed, when crossplotting logged P-wave velocity as a function of
280 resistivity (Figure 12), we can observe that the less altered granite have simi-
lar P-wave velocities but that their resistivity varies greatly (by a factor 100)
allowing to discriminate between the different alteration facies. Here also, the
challenge remains to deploy seismic techniques capable of remotely detecting

and imaging such anomalies.

285 **7. Conclusions**

Our study of an exhumed transition zone in the Vosges Mountain shows that altered porous and potentially permeable granite targeted in deep geothermal exploration has a clear signature on both electrical conductivity and seismic measurements that can be measured at core scale, borehole scale, and are still
290 visible with surface geophysical methods such as refraction and reflection seismic and Controlled Source Electromagnetism at a few hundred meter depth. It also showed that the best discrimination comes from the joint interpretation of these datasets. The challenge remains to develop and deploy electromagnetic and seismic imaging techniques having sufficient investigation depth and sufficient
295 resolution to detect and image the targets of interest, usually deeply buried underneath a thick sedimentary cover. A relevant strategy would be to combine both methods during exploration, in order to get benefit of the high sensitivity of resistivity to permeability with CSEM while conserving the high resolution of 3D seismic reflection.

300 **Acknowledgements**

The research leading to these results has received fundings from the French National Research Agency in the framework of the ANR project CANTARE-
Alsace under the grant agreement ANR-15-CE06-0014).
Large scale 3D EM modeling and inversion and P-wave tomography was per-
305 formed with BRGM's POLYEM3D code on the Occigen supercomputer thanks to GENCI (Grand Equipement de Calcul Intensif) and CINES (Centre Informatique National de l'enseignement Supérieur) supercomputing facilities.

References

- [1] C. Schmelzbach, S. Greenhalgh, F. Reiser, J.-F. Girard, F. Bretaudeau,
310 L. Capar, A. Bitri, Advanced seismic processing/imaging techniques and

their potential for geothermal exploration, *Interpretation* 4 (4) (2016) SR1–SR18.

- [2] C. M. Krawczyk, M. Stiller, K. Bauer, B. Norden, J. Henniges, A. Ivanova, E. Huenges, 3-d seismic exploration across the deep geothermal research platform groß schönebeck north of berlin/germany, *Geothermal Energy* 7 (1) (2019) 1–18.
- [3] A. D. Chave, A. G. Jones, *The magnetotelluric method: Theory and practice*, Cambridge University Press, 2012.
- [4] G. A. Newman, E. Gasperikova, G. M. Hoversten, P. E. Wannamaker, Three-dimensional magnetotelluric characterization of the coso geothermal field, *Geothermics* 37 (4) (2008) 369–399.
- [5] C. Arango, A. Marcuello, J. Ledo, P. Queralt, 3d magnetotelluric characterization of the geothermal anomaly in the llucmajor aquifer system (majorca, spain), *Journal of Applied Geophysics* 68 (4) (2009) 479–488.
- [6] S. Constable, Ten years of marine csem for hydrocarbon exploration, *Geophysics* 75 (5) (2010) 75A67–75A81.
- [7] F. Bretaudeau, S. Penz, N. Coppo, P. Wawrzyniak, M. Darnet, 3d land csem inversion in noisy environment with a single transmitter: inversion approach and application for geothermal water prospection, in: *International Symposium in Three-Dimensional Electromagnetics (3DEM)*, 2017.
- [8] M. Darnet, P. Wawrzyniak, N. Coppo, S. Nielsson, E. Schill, G. Fridleifsson, Monitoring geothermal reservoir developments with the controlled-source electro-magnetic method—a calibration study on the reykjanes geothermal field, *Journal of Volcanology and Geothermal Research* 391 (2020) 106437.
- [9] M. Darnet, N. Coppo, F. Bretaudeau, P. Wawrzyniak, S. Penz, B. Bourgeois, J.-C. Gourry, B. Sanjuan, Characterizing geothermal resources with passive and active electromagnetic methods in challenging em environments, in: *23rd Electromagnetic Induction Workshop: EMIW2016*, 2016.

- [10] R. L. Bruhn, W. T. Parry, W. A. Yonkee, T. Thompson, Fracturing and hydrothermal alteration in normal fault zones, *Pure and applied geophysics* 142 (3) (1994) 609–644.
- [11] J. Mercier, Structure et fonctionnement du milieu naturel en moyenne montagne–bassins de la petite fecht et du ringelbach (vosges, france), *Recherches Géographiques à Strasbourg* 19 (1982) 20–21.
- [12] B. Ambroise, J. Perrin, D. Reutenauer, Multicriterion validation of a semidistributed conceptual model of the water cycle in the fecht catchment (vosges massif, france), *Water Resources Research* 31 (6) (1995) 1467–1481.
- [13] J.-M. Baltassat, A. Legchenko, B. Ambroise, F. Mathieu, P. Lachassagne, R. Wyns, J. Mercier, J.-J. Schott, Magnetic resonance sounding (mrs) and resistivity characterisation of a mountain hard rock aquifer: the ringelbach catchment, vosges massif, france, *Near Surface Geophysics* 3 (4) (2005) 267–274.
- [14] T. Schaffhauser, F. Chabaux, B. Ambroise, Y. Lucas, P. Stille, T. Reuschlé, T. Perrone, B. Fritz, Geochemical and isotopic (u, sr) tracing of water pathways in the granitic ringelbach catchment (vosges mountains, france), *Chemical Geology* 374 (2014) 117–127.
- [15] R. Wyns, M. Tegye, étude géologique du cadre structural et des forages du bassin versant de recherche du ringlebach (sultzeren, haut-rhin), *Tech. Rep. BRGM/RP-56540-FR*, BRGM (French Geological Survey) (2012).
- [16] R. Wyns, J.-M. Baltassat, P. Lachassagne, A. Legchenko, J. Vairon, F. Mathieu, Application of proton magnetic resonance soundings to groundwater reserve mapping in weathered basement rocks (brittany, france), *Bulletin de la Société géologique de France* 175 (1) (2004) 21–34.
- [17] A. Belghoul, Caractérisation pétrophysique et hydrodynamique du socle cristallin, Ph.D. thesis, University of Montpellier II (2007).

- [18] A. Revil, L. Cathles III, S. Losh, J. Nunn, Electrical conductivity in shaly sands with geophysical applications, *Journal of Geophysical Research: Solid Earth* 103 (B10) (1998) 23925–23936.
- [19] R. Streich, M. Becken, O. Ritter, Robust processing of noisy land-based controlled-source electromagnetic data, *Geophysics* 78 (5) (2013) E237–E247.
- [20] P. WAWRZYNIAK, F. Smäi, Razorback, an open source python library for robust processing of magnetotelluric data, *Frontiers in Earth Science* 8 (2020) 296.
- [21] F. Bretaudeau, S. Penz, N. Coppo, P. Wawrzyniak, M. Darnet, Practical inversion of electric resistivity in 3d from frequency-domain land csem data, in: *23rd European Meeting of Environmental and Engineering Geophysics*, Vol. 1, European Association of Geoscientists & Engineers, 2017.
- [22] F. Bretaudeau, J. Porté, P. Wawrzyniak, S. Penz, B. Bourgeois, POLYEM3D: A massively parallel versatile code for 3d modeling and inversion of land csem and mt data, in: *Electromagnetic Induction Workshop, EMIW*, 2018.
- [23] F. Bretaudeau, F. Dubois, S.-G. Bissavetsy Kassa, N. Coppo, P. Wawrzyniak, D. M., Time-lapse resistivity imaging : Csem-data 3d double-difference inversion and application to the reykjanes geothermal field, *Geophysical Journal International* In Press.
- [24] R. Streich, 3d finite-difference frequency-domain modeling of controlled-source electromagnetic data: Direct solution and optimization for high accuracy, *Geophysics* 74 (5) (2009) F95–F105.
- [25] J. Nocedal, S. Wright, *Numerical optimization*, Springer Science & Business Media, 2006.

- [26] R.-E. Plessix, W. Mulder, Resistivity imaging with controlled-source electromagnetic data: depth and data weighting, *Inverse problems* 24 (3) (2008) 034012.
- 395 [27] J.-M. Baltassat, B. Ambroise, F. Mathieu, Boucher, M., R. Wyns, Réinterprétation des investigations géophysiques du bassin versant du ringelbach à l'aide des données de forage et des mesures sur échantillon en laboratoire, Tech. Rep. BRGM/RP-66694-FR, BRGM (French Geological Survey) (2018).
- 400 [28] M. H. Waxman, L. Smits, et al., Electrical conductivities in oil-bearing shaly sands, *Society of Petroleum Engineers Journal* 8 (02) (1968) 107–122.
- [29] P. N. Sen, P. A. Goode, Influence of temperature on electrical conductivity on shaly sands, *Geophysics* 57 (1) (1992) 89–96.
- 405 [30] C. Glaas, A. Genter, J. Girard, P. Patrier, J. Vidal, How do the geological and geophysical signatures of permeable fractures in granitic basement evolve after long periods of natural circulation? insights from the ritter-shoffen geothermal wells (france), *Geothermal Energy* 6 (1) (2018) 14.

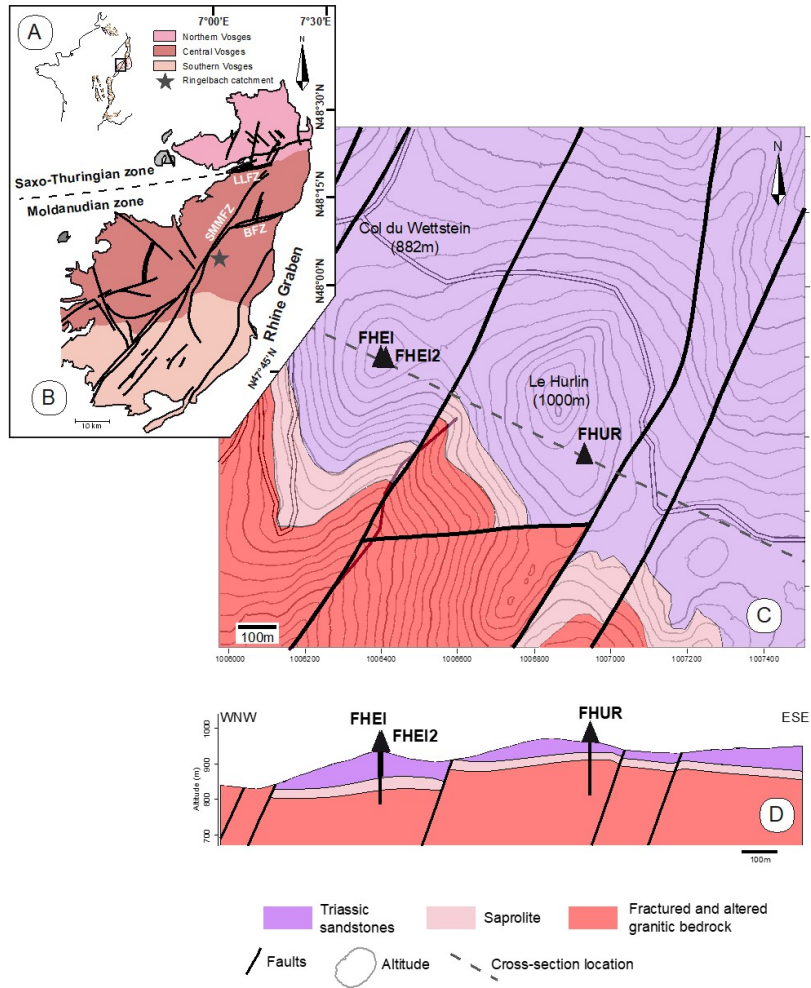
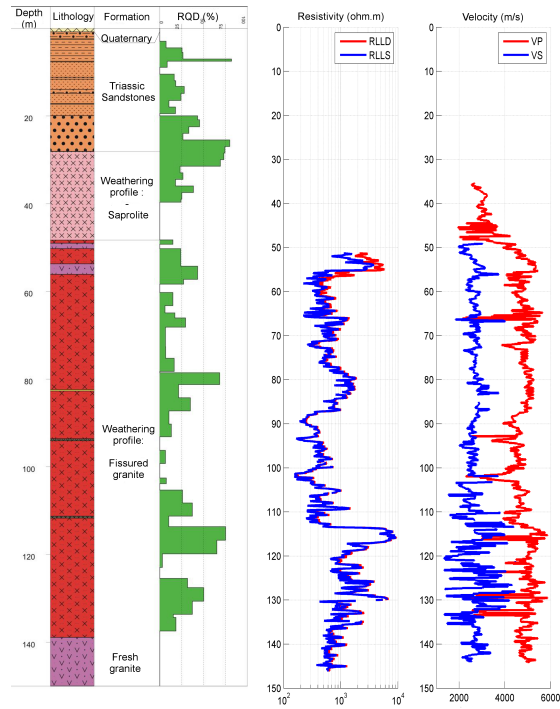
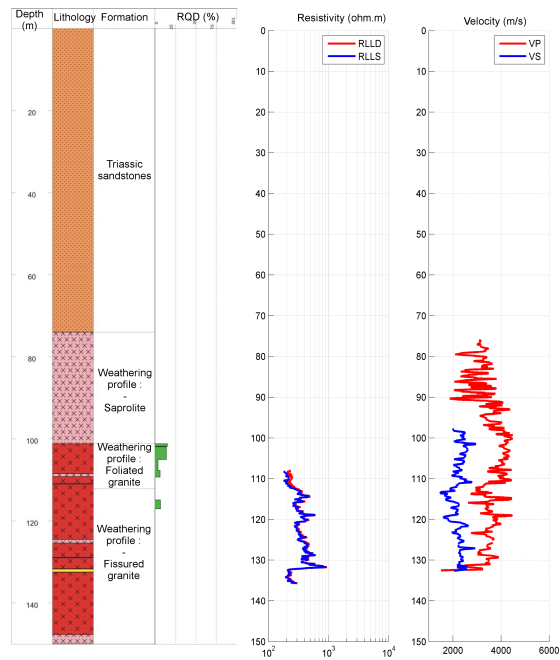


Figure 1: Geological setting of the Ringelbach catchment. A- The European Cenozoic Rift System in France and the location of the Vosges massif as western shoulder of the rift. B- Simplified map of the Vosges massif. LLFZ: Lalaye-Lubine Fault Zone; SMMFZ: Saint Marie aux Mines Fault Zone; BFZ: Bilstein Fault Zone. C- Topographic and geologic map of the Ringelbach catchment with the location of the boreholes (triangles). D – Cross-section through the boreholes.

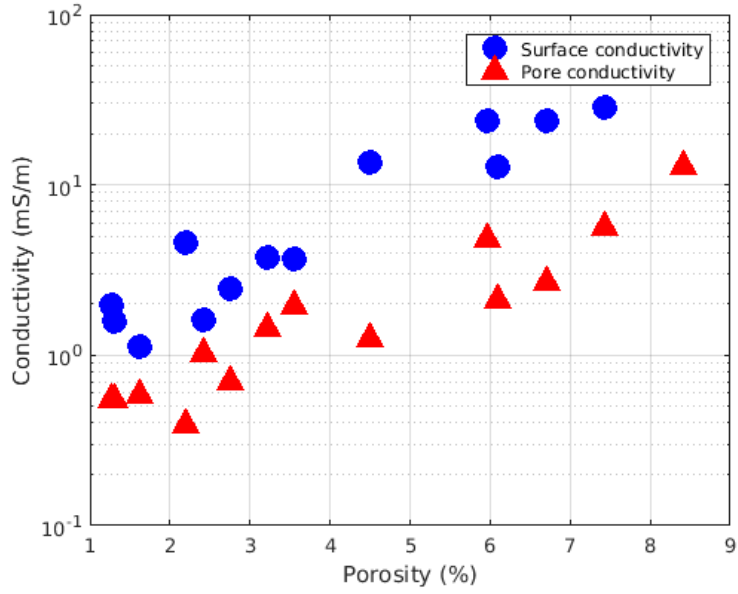


(a) F-HUR borehole

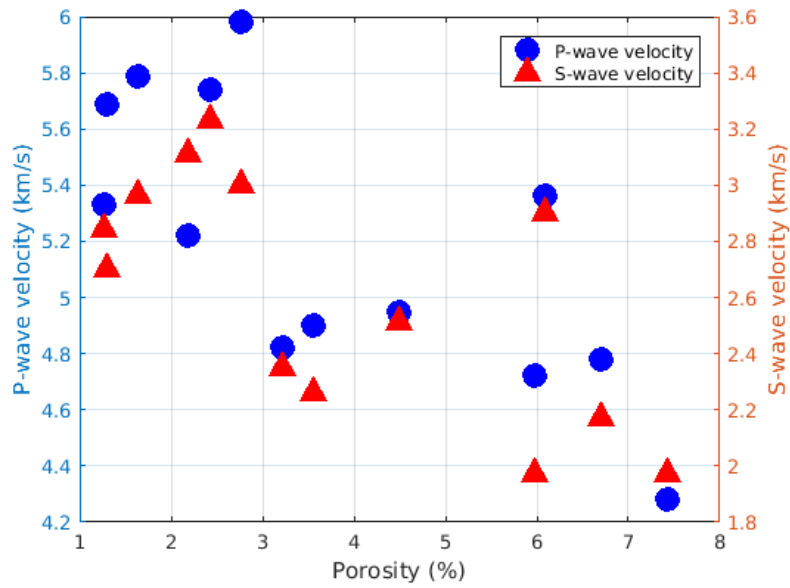


(b) F-HEI borehole

18
 Figure 2: Lithological, RQD, logged resistivity and sonic velocity profiles of F-HEI (a) and F-HUR (b). RQD log is a proxy for the competency of the rock.



(a) Surface and pore conductivity versus porosity



(b) P-wave velocity versus porosity

Figure 3: Variation with porosity of surface and pore conductivity (a) and P-wave velocity (b) of altered granite core samples extracted from the Ringelbach transition zone [17].

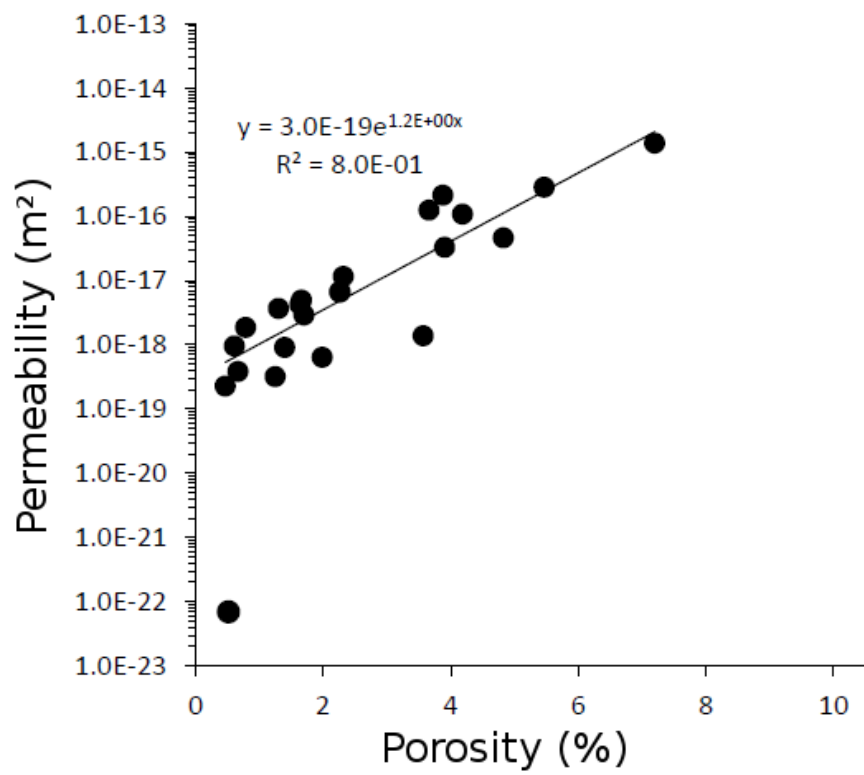


Figure 4: Permeability as a function of the porosity from Ringelbach's core samples [17].

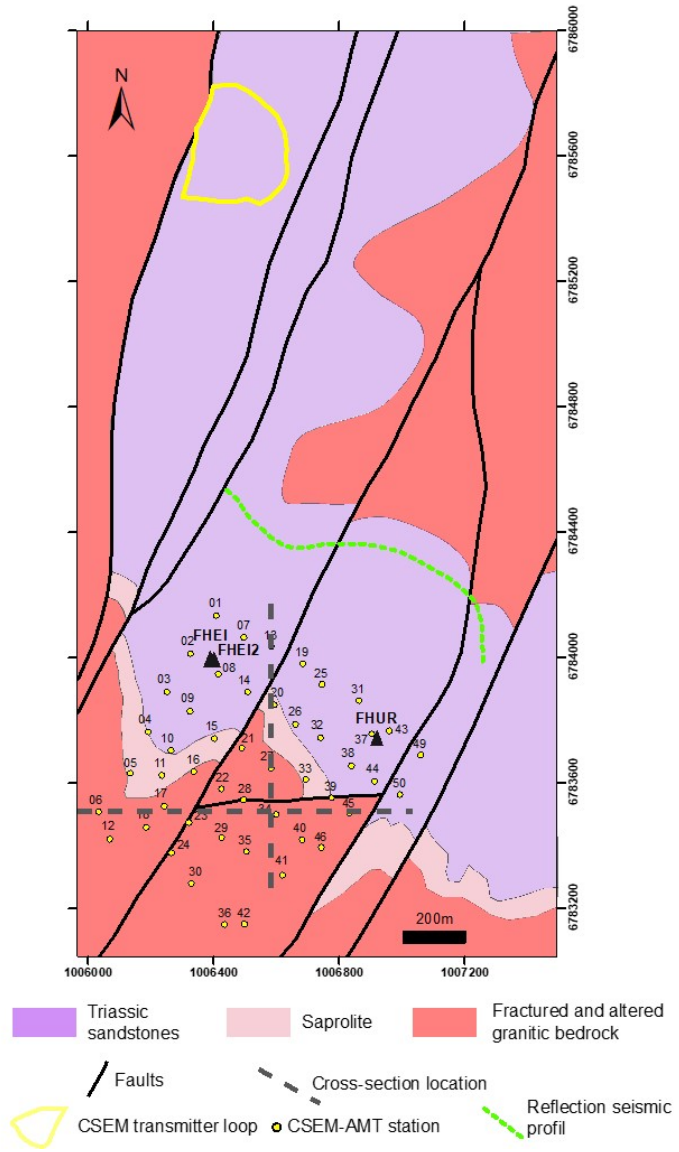


Figure 5: Location of the 3D CSEM grid (measurement station and transmitter loop in yellow), the reflection/refraction seismic profile (green line) and the boreholes (F-HEI, F-HUR). Background is the geological map of the area.

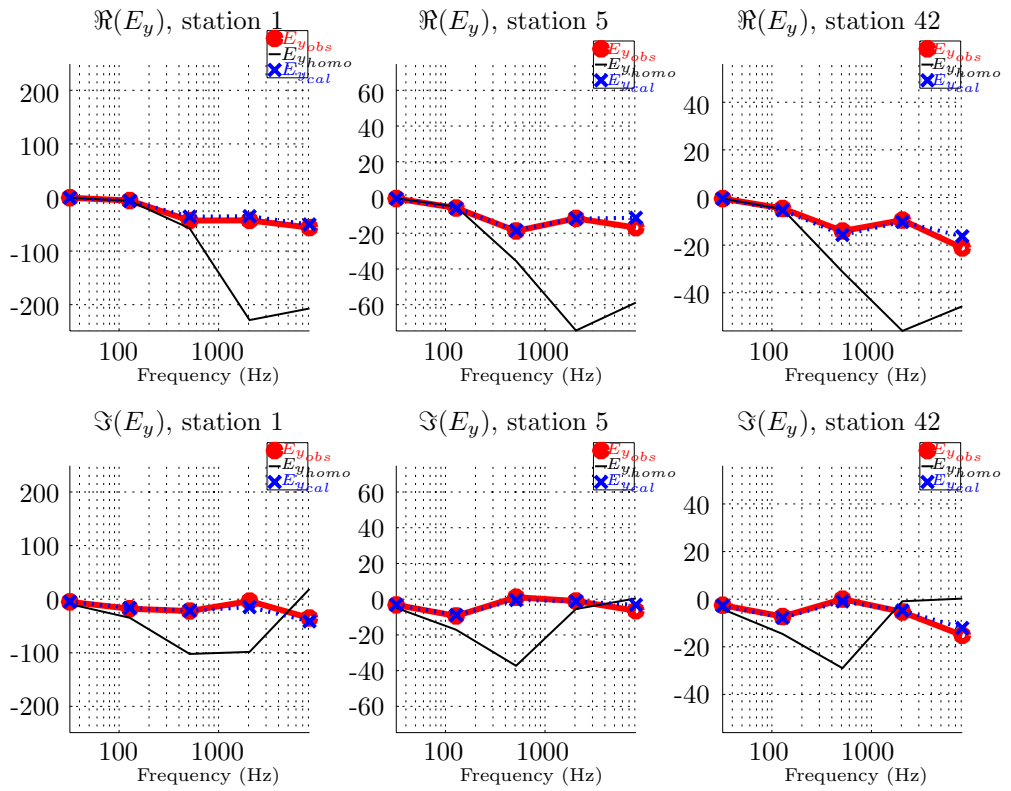


Figure 6: Example of data spectra. Real and imaginary parts of the electric field (in nV/km) as a function of frequency.

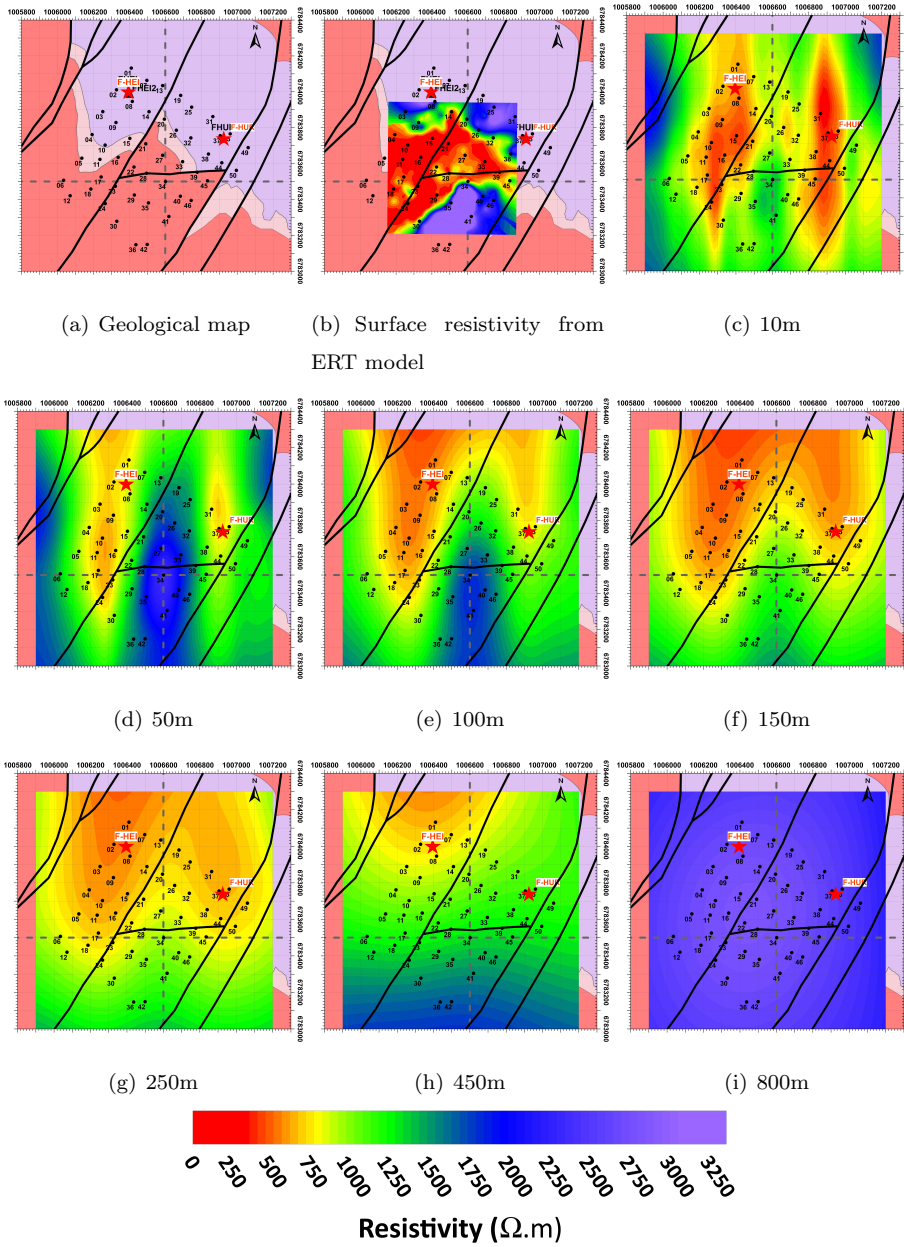


Figure 7: Resistivity slices at different depth from the cube obtained from the inversion of 3D Controlled-Source Electro-Magnetic data over the Geological map.

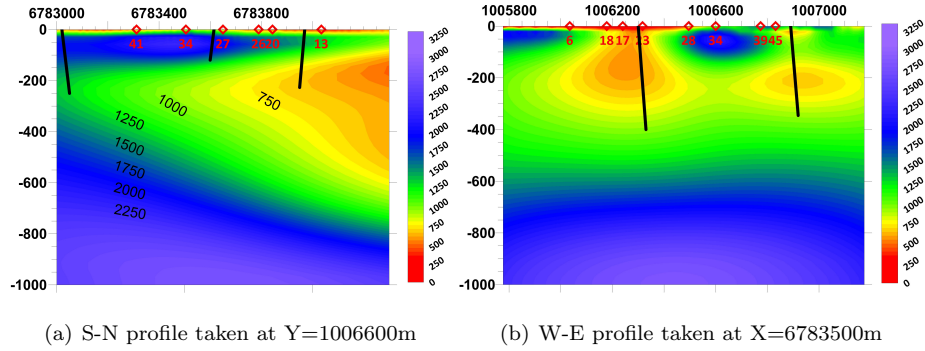


Figure 8: S-N (a) and W-E (b) resistivity profiles from the cube obtained from the inversion of 3D Controlled-Source Electro-Magnetic data

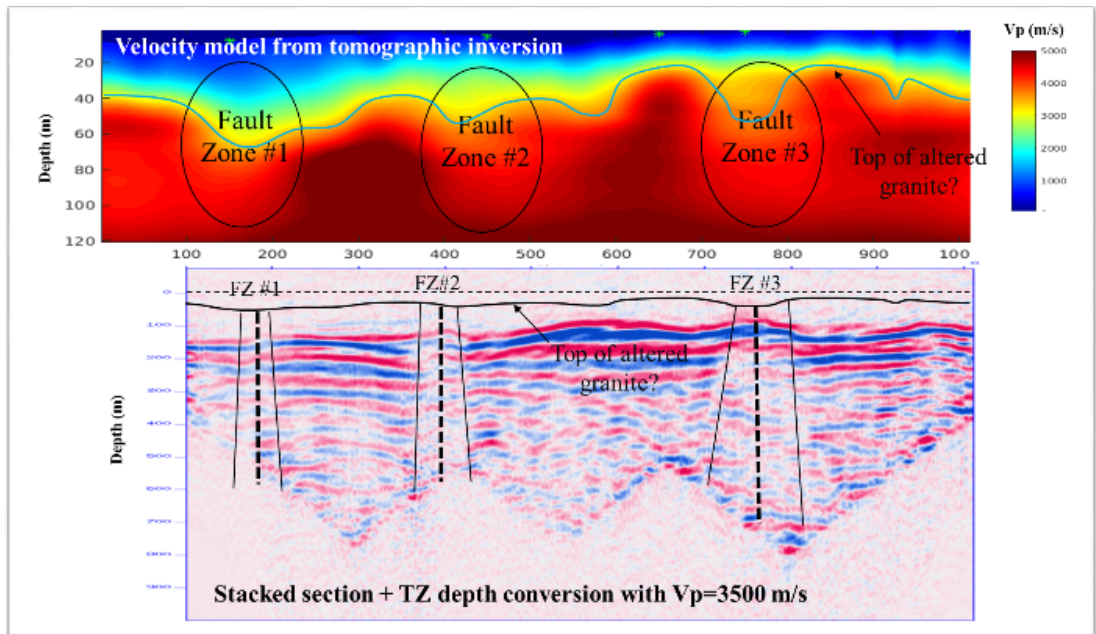


Figure 9: Top: Velocity model derived from the first arrival traveltimes tomography. Bottom: constant velocity stacked migrated section in depth. The footprint of the faults is visible in the tomography section with a velocity drop and in the reflection profile with a loss of coherency in the reflector.

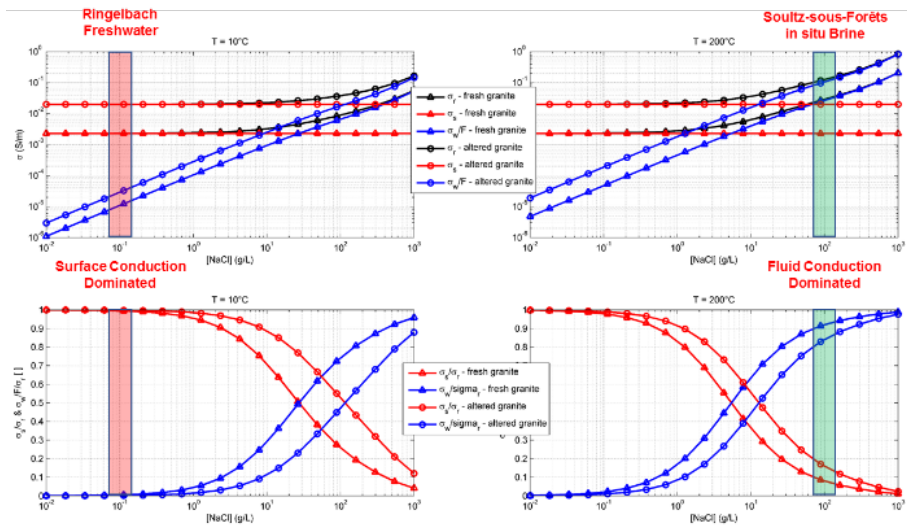


Figure 10: Top left: surface (red), pore fluid (blue) and total (black) conductivity of unaltered (triangle) and altered (circle) granite at 10 degC as a function of the brine salinity. Bottom left: ratio between the surface (red) and pore fluid (blue) versus the total rock conductivity for fresh (triangle) and altered (circle) granite at 10 degC as a function of the brine salinity. Top right: surface (red), pore fluid (blue) and total (black) conductivity of unaltered (triangle) and altered (circle) granite at 200 degC as a function of the brine salinity. Bottom right: ratio between the surface (red) and pore fluid (blue) versus the total rock conductivity for fresh (triangle) and altered (circle) granite at 200 degC as a function of the brine salinity.

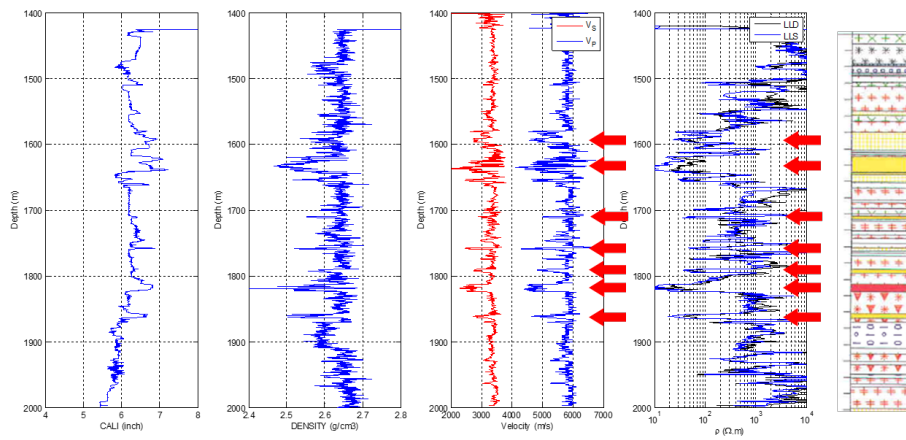


Figure 11: P-wave (blue) and S-wave (red) logs (left), shallow (blue) and deep (black) laterolog (middle) and lithological log (right) in the Soultz-sous-Forêts GPK1 well. Most altered granitic facies are marked with red arrows.

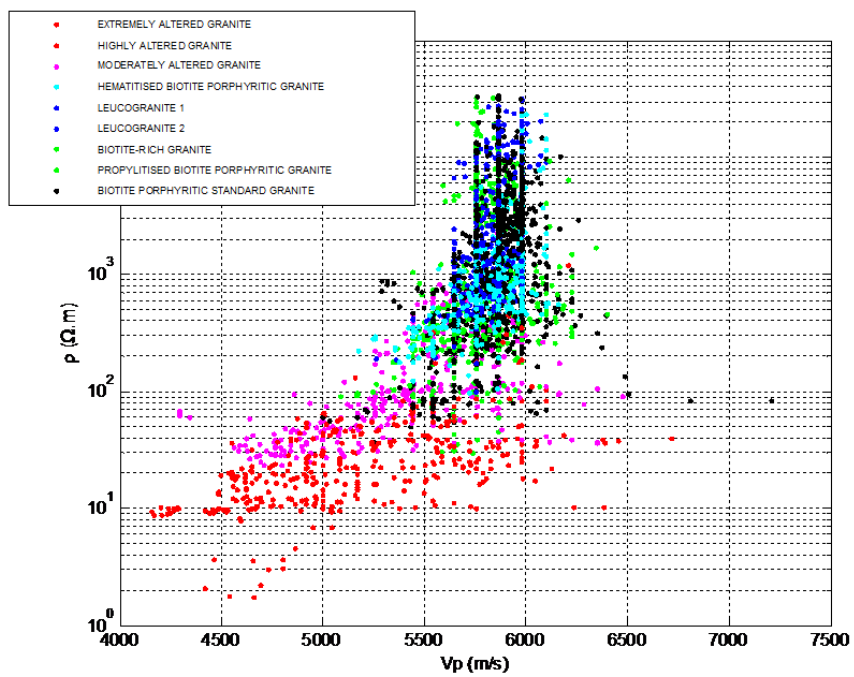


Figure 12: Logged resistivity as a function of the P-wave velocity of the granitic basement found in the Soultz-sous-Forêts GPK1 well. Colors indicate the different alteration facies.